



1 **Diurnal cycle of iodine and mercury concentrations in Svalbard surface snow**

2 ¹Andrea Spolaor, ¹Elena Barbaro, ²David Cappelletti, ¹Clara Turetta, ³Mauro Mazzola, ⁴Fabio Giardi,
3 ⁵Mats P. Björkman, ⁶Federico Lucchetta, ¹Federico Dallo, ⁷Katrine Aspö Pfaßhuber, ⁸Hélène
4 Angot, ⁹Aurelien Dommergue, ¹⁰Marion Maturilli, ¹¹Alfonso Saiz-Lopez, ^{6,1}Carlo Barbante and
5 ¹Warren RL Cairns

6
7 ¹*Institute for the Dynamics of Environmental Processes, IDPA-CNR, Campus Scientifico Via Torino*
8 *155, 30172 Mestre, Venice, Italy.*

9 ²*Dipartimento di Chimica, Biologia e Biotecnologie, Università degli Studi di Perugia I-06123*
10 *Perugia, Italy*

11 ³*National Research Council, Institute of Atmospheric Sciences and Climate, CNR-ISAC, Via P.*
12 *Gobetti 101, Bologna, Italy*

13 ⁴*Chemistry Department – Analytical Chemistry, Scientific Pole, University of Florence, Via della*
14 *Lastruccia 3, I-50019 Sesto Fiorentino (Florence) Italy.*

15 ⁵*University of Gothenburg, Department of Earth Sciences, Box 460, 40530 Göteborg, Sweden*

16 ⁶*Ca' Foscari University of Venice, Department of Environmental Sciences, Informatics and Statistics,*
17 *Santa Marta – Dorsoduro 2137, 30123 Venice, Italy.*

18 ⁷*NILU - Norwegian Institute for Air Research, Kjeller, Norway*

19 ⁸*Institute of Arctic and Alpine Research (INSTAAR), University of Colorado, Boulder, USA*

20 ⁹*Institut des Géosciences de l'Environnement, Univ. Grenoble Alpes /CNRS, F 38041 Grenoble,*
21 *France.*

22 ¹⁰*Alfred Wegener Institute, Helmholtz Centre for Polar and Marine Research, Potsdam, Germany*

23 ¹¹*Department of Atmospheric Chemistry and Climate, Institute of Physical Chemistry Rocasolano,*
24 *CSIC, Madrid, Spain*

25

26

27

28

29

30

31

32

33

34

35

36



37 **Abstract**

38 Sunlit snow is highly photochemically active and plays an important role in the exchange of gas-
39 phase species between the cryosphere to the atmosphere. Here, we investigate the behaviour of two
40 selected species in surface snow: mercury (Hg) and iodine (I). Hg can deposit year-round and
41 accumulate in the snowpack. However, photo-induced re-emission of gas phase Hg from the surface
42 has been widely reported. Iodine is active in atmosphere new particle formation, especially in the
43 marine boundary layer, and in the destruction of atmospheric ozone. It can also undergo
44 photochemical re-emission. Although previous studies indicate possible post-depositional processes,
45 little is known about the diurnal behaviour of these two species and their interaction in surface snow.
46 The mechanisms are still poorly constrained and no field experiments have been performed in
47 different seasons to investigate the magnitude of re-emission processes. Three high temporal
48 resolution (hourly samples) 3 days long sampling campaign were carried out near Ny-Ålesund
49 (Svalbard) to study the behaviour of mercury and iodine in surface snow under different sunlight and
50 environmental conditions (24h-darkness, 24h-sunlight and day/night cycles). Our results indicate a
51 clearly different behaviour of Hg and I in surface snow during the different campaign. The day/night
52 experiments demonstrate the existence of a diurnal cycle in surface snow for Hg and iodine, indicating
53 that these species are indeed influenced by the daily solar radiation cycle. Differently bromine did
54 not show any diurnal cycle. The diurnal cycle disappeared also for Hg and iodine during the 24h-
55 sunlight period and during 24h-darkness experiments supporting the idea of the occurrence (absence)
56 of a continuous recycling/exchange at the snow-air interface. These results demonstrate that this
57 surface snow recycling is seasonally dependent, through sunlight. They also highlight the non-
58 negligible role that snowpack emissions have on ambient air concentrations and potentially on iodine-
59 induced atmospheric nucleation processes.

60
61
62
63
64
65
66
67
68
69
70
71
72



73 **1. Introduction**

74 Polar Regions are being increasingly studied for their important roles in global climate and
75 atmospheric chemical cycles. Multiple studies have improved our understanding of atmospheric
76 processes in polar regions, ranging from new particle formation processes (Dall'Osto et al., 2017;
77 Sipilä et al., 2016), ozone destruction processes (Saiz-Lopez et al., 2007; Simpson et al., 2007), the
78 role of halogens in polar atmospheric processes (Saiz-Lopez and von Glasow, 2012; Spolaor et al.,
79 2013a), the mercury cycle (Angot et al., 2016a; Aspmo et al., 2005; Dommergue et al., 2003a;
80 Durnford and Dastoor, 2011) to atmospheric transport and deposition of natural and anthropogenic
81 compounds (Moroni et al., 2015; Moroni et al., 2017; Udisti et al., 2016; Zangrando et al., 2013). The
82 Polar Regions are characterized by periods with 24 h of continuous solar radiation (April to
83 September in the Arctic), periods when the night and day cycle is present (February to March and
84 September to October in the Arctic) and periods of continuous darkness (November to January in the
85 Arctic), the so-called polar night. The different periods have completely different environmental
86 conditions depending on the incoming solar radiation, with variables such as sea ice presence or
87 biological activity being radically altered by sunlight. One important aspect is snow cover. Annual
88 snow is present, on average, for almost nine months of the year and represents an important
89 environmental component of Polar Regions. In Svalbard, the snow starts to accumulate in October
90 and remains until the end of May when the melting season begins (Førland et al., 2011). However,
91 with Arctic temperatures rising (Maturilli et al., 2013), the length of the snow cover has diminished
92 (Brage B. Hansen et al., 2014), with direct consequences on the environment of the Svalbard
93 archipelago, such as glacier mass loss, permafrost thawing, disturbances of the local fauna etc.
94 (Karner et al., 2013; Kohler and Aanes, 2004; Kohler et al., 2007; Westermann et al., 2011). The
95 annual snow layer is an extremely dynamic portion of the cryosphere, and can be defined as the snow
96 accumulated and present on the ground during the whole year (Spolaor et al., 2016a). The
97 characteristics of the annual snow strata are strongly dependent on climate conditions and may
98 influence food access for animals that rely on food sources below the snow (Kohler and Aanes, 2004).
99 From a chemical point of view, snow is a sink for an impressive number of chemical compounds
100 (natural and anthropogenic) and elements (Björkman et al., 2013; Gabrieli et al., 2011; Vecchiato et
101 al., 2018). Specific compounds and elements accumulate during the winter can undergo photo-
102 activation and can be re-emitted into the atmosphere (Angot et al., 2016c; Spolaor et al., 2014), while
103 taking part in numerous geochemical and biological cycles (Björkman et al., 2014) during spring and
104 summer. Mercury (Hg) and iodine (I) are two elements that can be photo activated and released from
105 the snow pack. Mercury is a heavy metal with a known toxicity present in the environment in several
106 different chemical forms. It is reactive in the environment and undergoes photochemical reactions
107 that change its speciation and chemical behaviour (Dommergue et al., 2010; Durnford and Dastoor,
108 2011; Saiz-Lopez et al., 2018; Steffen et al., 2002). Mercury in its oxidized form can be deposited



109 onto the snowpack, increasing Hg concentrations in the upper snow strata (Obrist et al., 2017). Once
110 present in the snowpack, Hg is very labile, and it can be reduced back to elemental Hg (Hg(0)) and
111 undergo dynamic exchange with the atmosphere above (Song et al., 2018; Spolaor et al., 2018;
112 Steffen et al., 2002). The role of the snowpack is crucial in the mercury cycle in Polar Regions since
113 it acts as both a sink (deposition, accumulation) and a source (re-emission). Several studies have
114 already been carried out in the polar regions with the aim of determining the extent of mercury
115 recycling between the surface snow and the lower atmosphere (Angot et al., 2016c; Brooks et al.,
116 2008; Dommergue et al., 2012; Douglas et al., 2008; Han et al., 2014; Obrist et al., 2017; Wang et
117 al., 2016). It has been shown that surface Arctic snow could lose up to 90 % of its total Hg content
118 within 48 hours (Poulain et al., 2004). Similar, re-emission/loss rates of Hg from snow surface (35–
119 50 %) and drifting snow (65–75 %) over 10.5 h have been suggested in chamber experiments
120 (Sherman et al., 2010) while, in a study performed on the Antarctic Plateau, Spolaor et al. 2018
121 suggest a loss of 90% of mercury in the upper snow layer within a few hours.

122 Similar to mercury, iodine can undergo photochemical activation in surface snow resulting in its
123 presence in the surrounding atmosphere (Frieb et al., 2010; Spolaor et al., 2014). Several studies
124 aimed at understanding the behaviour of iodine in the Arctic region, from a paleo perspective using
125 ice core archives (Cuevas et al., 2018; Spolaor et al., 2016b), and field (atmospheric and snow)
126 experiments (Frieb et al., 2010; Gilfedder et al., 2007). The role of iodine in new particle formation
127 as well in ozone destruction is currently under investigation (Allan et al., 2015; Saiz-Lopez et al.,
128 2012; Saiz-Lopez, 2006; Sipilä et al., 2016) since it could have a direct effect on the radiative budget
129 of polar areas. Up to now, it was believed that iodine was mainly associated with biological emissions,
130 however, recent studies have underlined the increase in ocean inorganic emissions (tripled since 1950)
131 connected with the increase in anthropogenic ozone via reactions over the ocean surface (Cuevas et
132 al., 2018). Like mercury, iodine could be released from surface snow and directly participate in
133 specific processes within the marine boundary layer, particularly in new particle formation. Little
134 information exists on the behaviour of mercury and iodine in surface snow during different seasons.
135 Laboratory experiments have been carried out to understand light-induced processes regarding Hg
136 and iodine (Durnford and Dastoor, 2011; Saiz-Lopez et al., 2012; Spolaor et al., 2013b). However
137 few experiments have been carried out in the field, with the specific aim of understanding the diurnal
138 dynamics of these elements in surface snow (Dommergue et al., 2003b; Ferrari et al., 2005; Spolaor
139 et al., 2018). The unique high-temporal resolution experiments presented, aim to improve our
140 understanding of the behaviour of these elements in the upper snow layers (0-3 cm) under different
141 light and atmospheric conditions to investigate their short-term (diurnal) variation.

142

143 2. Methods



144 The experiments were conducted in the vicinity of Ny-Ålesund, in the snowfield behind the
145 Gruvebadet aerosol site (Figure 1). This area has a homogeneously flat surface without specific
146 elevation changes or obstacles that might interfere with snow deposition or wind-blown redistribution.
147 This area is approximatively 1 km from the coast line of the Kongsfjorden and about 400 m from the
148 Zeppelin mountain. The “Gruvebadet” snow field is located to the south of Ny-Alesund at an
149 elevation of the 80 m a.s.l. (Figure 1). Atmospheric mercury concentrations were obtained from the
150 Zeppelin Observatory located at 474 m a.s.l. The “Gruvebadet” snow field is located to the south of
151 Ny-Ålesund, while the prevailing wind are mainly from east and south-east, minimizing possible
152 influences from station activities.

153

154 **2.1 Sampling period and strategy**

155 Surface snow samples were collected in the vicinity of Ny-Ålesund, specifically in the snow field
156 behind the “Gruvebadet” Aerosol Laboratory (Figure 1). Three experiments were conducted, two in
157 spring (2015 and 2016) and one in winter (2017). In 2015, we performed the first surface experiment
158 (hereafter called the “2015 experiment”) between the 28th of April and the 1st of May. This period
159 was characterized by 24 hours of sunlight (incoming solar radiation ranged from a minimum of 25
160 Wm^{-2} to a maximum of 456 Wm^{-2}). In 2016, a second experiment (hereafter called the “2016
161 experiment”) was carried out between the 6th and the 9th of April when the night and day cycle was
162 still present at Ny-Ålesund (incoming solar radiation between 0 and 227 Wm^{-2}). The last experiment
163 was conducted during the polar night, between the 24th and the 29th of January 2017 (hereafter called
164 the “2017 experiment”) with the complete absence of incoming solar radiation. To determine the
165 diurnal variation, and the rates of the expected changes in iodine and mercury concentrations, a high
166 temporal resolution (hourly) sampling strategy was adopted. An area of approximately 2 m x 2 m was
167 delimited for surface snow sampling, and all samples were collected inside this delimited area. At the
168 beginning of the experiment, six samples were collected to evaluate the spatial variability of mercury,
169 iodine, bromine (bromine is limited to the “2016 experiment”) and sodium in surface snow within
170 the delimited snowfield. Afterwards, surface snow (the first 3 cm) was sampled with an hourly
171 resolution for three consecutive days. The upper 3 cm were chosen as this is the snow layer that is
172 most influenced by the surrounding atmospheric conditions, and, in case of snowfall, by deposition
173 (Spolaor et. al. 2018). During snow sampling, the temperature of surface snow was also measured.
174 To minimize spatial variability, samples were collected following a straight line leaving about 5 cm
175 between each of the sampling points. After collection, the snow samples were stored at -20°C in dark
176 conditions and transported to the Venice IDPA-CNR laboratories. The samples were never melted or
177 exposed to direct sunlight until analysis.

178

179 **2.2 Meteorological measurements**



180 Meteorological and radiation conditions were monitored at the Amundsen-Nobile Climate Change
181 Tower (Mazzola et al., 2016), located about 500 m west of the sampling site and from the AWIPEV
182 observatory (Maturilli et al., 2013), located about 800 m north of the sampling site. No meteorological
183 measurements are present in the sampling area. Temperature, relative humidity, were measured at 2
184 m above ground level and were considered as representative of the atmosphere just above the snow
185 surface while wind speed and direction at 10 m above ground. Incoming solar radiation was measured
186 at the top of the CCT tower (33 m), this value was not influenced by reflections from the structure.
187 One-minute data were used to obtain hourly averages. Snow accumulation data were obtained by
188 measuring the high of 4 plastic poles located at the extremities of the snow sampling field.
189 Precipitation data were recorded in Ny-Ålesund by the Norwegian Meteorological Institute (station
190 n. 99910) and downloaded through the eKlima database (eklima.no).

191

192 **2.3 Snow Mercury analysis**

193 Total Hg concentrations in surface snow samples was determined using a Thermo Element
194 Inductively Coupled Plasma Sector Field Mass Spectrometry (ICP-SFMS Element XR, Thermo-
195 Fisher, Bremen, Germany) in low resolution scanning mode using ^{202}Hg as the analytical mercury
196 mass with 10 replicates per sample measurement. The instrument was calibrated using standards
197 prepared from a mono-elemental Hg solution (TraceCert®, purity grade, Sigma-Aldrich, MO, USA).
198 Hg calibration standards were re-analysed every 10 samples as a quality control check. The percent
199 relative standard deviation ($n=10$) ranged from 0.5 % at 500 pg g^{-1} to 10 % at 1 pg g^{-1} and amounted
200 to 2.6 % on average. Considering the high volatility and instability of Hg in solution, the samples
201 were acidified at 2 % v/v with ultrapure hydrochloric acid before they were melted and analyzed.
202 Each sample was weighed and the exact amount of HCl was added to reach a final concentration of
203 2 % (Planchon et al., 2004; Spolaor et al., 2018).

204

205 **2.4 Snow iodine, sodium and bromine analysis**

206 Halogens (I and Br) and sodium analyses were conducted on non-acidified samples. Total sodium
207 (Na), iodine (I) and bromine (Br) concentrations were determined by ICP-SFMS (Spolaor et al.,
208 2016c). Each analytical run started and ended with an ultra-pure water (UPW) cleaning session of 3
209 min to ensure a stable background level throughout the analysis. The external standards that were
210 used to calibrate the analytes were prepared by diluting a 1000 ppm stock IC (ion chromatography)
211 standard solution (TraceCERT® purity grade, Sigma-Aldrich, MO, USA). The standard
212 concentrations ranged between 10 and 4000 ng g^{-1} for sodium, 0.01 and 1 ng g^{-1} for iodine and between
213 0.5 and 20 ng g^{-1} for bromine. The residual standard deviation (RSD) was low for all analytes, the
214 halogens ranged between 1–2% and 2–5% for Br and I, respectively, and the RSD was 3–4 % for
215 sodium.



216 **2.5 Atmospheric mercury measurements**

217 Gaseous elemental mercury (GEM) was monitored using a Tekran 2537 Hg vapor analyzer as
218 described by Aspö et al., 2005 and as summarized here: ambient air was sampled at 1.5 l min^{-1}
219 through a Teflon filter via a heated sampling line. A soda-lime trap was mounted in-line before the
220 instrument filter. Hg in the air is pre-concentrated for 5 minutes by amalgamation on two parallel
221 gold cartridges, which alternate between collection and thermal desorption, followed by AFS (atomic
222 fluorescence spectrometric) detection. The instrument was auto-calibrated every 25 hours using an
223 internal Hg permeation source, whose accuracy was verified during routine site audits that include
224 manual injections of Hg from an external source (Aspö et al., 2005).

225 **3. Results**

226 The 2015 and 2016 experiments were characterized by similar atmospheric conditions (except for the
227 incoming solar radiation) while during the 2017 experiment a storm approached Ny-Ålesund during
228 the first 12 hours of the experiment with strong winds lasting for the first 24 hours of the experiment.
229 During the 2015 experiment under full day conditions, the average air temperature ranged between -
230 10°C and -6°C and the surface snow temperature range between -13°C and -5°C , showing a diurnal
231 variability connected with changes in the incoming solar radiation (Figure 2). Incoming solar
232 radiation ranged from a minimum of 25 Wm^{-2} to a maximum of 450 Wm^{-2} . Wind speed was almost
233 constant and remained below 3 ms^{-1} during most of the experiment, except for a few hours at the
234 beginning when it exceeded 3 ms^{-1} . Snowfall (1 cm net accumulation on the ground) occurred on the
235 30th of April between 3 am and 11 am (Figure 2, pink rectangle). A snow event, causing a net
236 accumulation of 1 cm of snow, also occurred during the 2016 experiment (Figure 3, pink rectangular)
237 when day and night periods were present. The snow event occurred on the 9th of April between 10
238 am and 3 pm. During the 2016 experiment, conducted between 6th and the 9th of April, the snow
239 temperature was not registered due a technical problem with the temperature probe installed in the
240 snow. Air temperature ranged between -7 and -3°C and solar radiation between zero at night time to
241 a maximum of 227 W/m^2 . As for the first experiment, wind speed was below 3 ms^{-1} , minimizing the
242 effect of blowing snow. Wind direction was almost constant and prevailing from east. The GEM and
243 the surface snow mercury datasets were de-trended to emphasize the diurnal variation and remove
244 the decreasing trend present in both datasets. The de-trended series were obtained calculating the
245 linear regression line for both series and subtracting this value from the data. Figure 3 (middle panel)
246 reports the de-trended mercury dataset while the Figure 4 shows the raw data and the methods used
247 to remove the trend. The 2017 winter experiment (Figure 5) was characterized by a snowstorm that
248 occurred on the 24th of January (10 hours after the experiment began, pink rectangle). Differently to
249 the previous experiments, the wind speed averaged 9 ms^{-1} during the storm, with a maximum speed
250 of 16 ms^{-1} (Figure 5, orange line). Strong winds can redistribute surface snow and significantly



251 change chemical concentrations. For these reasons, the winter experiment began on the 24th of
252 January and ended on the 29th of January for 5 days in total, compared the 3 days adopted for the
253 2015 and 2016 experiment. The length of the experiment was extended of 2 days to minimize the
254 impact of the strong wind and snowfall that occurred at the beginning of the experiment. Air
255 temperatures ranged from between -17°C and -3°C, while snow temperatures ranged between -25°C
256 and -10°C (Figure 5, upper panel). One important issue that could confound the results obtained by
257 surface sampling is spatial variability. Spatial variability was tested during the three experiments and
258 specifically for the four elements investigated. Six surface snow aliquots were collected at the
259 beginning of each experiment within the delimited area at the same time. The results obtained show
260 that for sodium, bromine and mercury, spatial variability can explain 10% of the variability whilst
261 for iodine the variability was of the order of 5%. Concentrations detected during the three experiments
262 show different background levels (Table 1) for total iodine, sodium, mercury and gaseous elemental
263 mercury (Br was measured only during the 2016 experiment). For sodium, the highest concentration
264 was detected during the 2015 (full day) experiment where concentrations in surface snow averaged
265 3500 ngg⁻¹. The lowest sodium concentrations were determined during the winter period with
266 concentrations of around 1500 ngg⁻¹. For iodine the trend was the opposite, with highest
267 concentrations in winter (0.38 ngg⁻¹) and the lowest during the 24h sunlight period (0.15 ngg⁻¹). For
268 total mercury, the minimum concentration was found in early spring (0.007 ngg⁻¹, 2016 experiment)
269 while the highest values were detected during 2015 (full light) and 2017 winter experiment (on
270 average 0.010 ngg⁻¹ for 2015 and 0.009 ngg⁻¹ for 2017). Gaseous elemental mercury has the highest
271 concentration during springtime, when 24 h incoming solar radiation is present (1.45 ngm⁻³) while
272 the lowest value has been detected during polar night (1.28 ngm⁻³). The average concentration during
273 the experiment is only representative for specific periods in the experiment and should not be
274 considered as a reference concentration for a specific season. However, some indications emerged,
275 especially for iodine, which showed the highest concentrations during the polar night in the absence
276 of solar radiation. Considering iodine (inorganic and organic) is mainly emitted by oceanic processes,
277 iodine concentrations were normalized to sodium concentrations to obtain an iodine enrichment (I_{enr})
278 compared to the bulk seawater abundance. This is defined as $I_{\text{enr}} = I_{\text{snow}} \times (\text{Na}_{\text{snow}} / [\text{I/Na}]_{\text{sw}})$, where I/Na
279 = 0.00000596, (Millero et al., 2008) where “sw” = measured sea water abundance. In the 2015
280 experiment (24h sunlight), iodine had an average enrichment value of 5, a value that exponentially
281 increased (up to 190) during snowfall (Figure 2), so if we consider the snowfall period the mean value
282 increases to 10. The 2016 experiment (day/night) was characterized by a diurnal cycle for both
283 mercury and iodine (and I_{enr}) and by an average I_{enr} value of 11, with the lowest value during day
284 time and higher values detected during the night periods (Figure 3). As for the 2015 experiment, the
285 experiment conducted in 2016 was characterized by a snowfall event that significantly influenced the
286 surface iodine concentration and its enrichment factor. During the 2016 experiment, snowfall caused



287 the I_{enr} to increase up to 300. The rapid increase in iodine and its enrichment factor during snowfall
288 was followed by a rapid decrease to the pre-snowfall (seasonal background value) concentration
289 during the 2015 experiment (Figure 2), whilst in the 2016 experiment the increased concentration and
290 enrichment caused by the snow fall was most likely masked by the night time deposition (Figure 3).
291 Similar behaviour was measured for total mercury in surface snow samples, with an increase in
292 concentration during snowfall followed by a rapid decrease in both experiments (Figure 2 and 3). The
293 winter experiment is characterized by the highest iodine enrichment values (47 on average) and,
294 similar the previous experimental results, the experiment was characterized by snowfall and strong
295 winds during the first 24h. During the storm period in the winter experiment we detected an increase
296 in iodine concentrations (and I_{enr} up to 100), however the difference in iodine enrichment between
297 the snowfall periods and rest of samples collect was not statistically significant. The average
298 elemental concentrations for each experiment are reported in Table 1.

299

300 4. Discussion

301 The behaviour of mercury and iodine in surface snow depends on the season and the amount of
302 incoming solar radiation (Figure 2, Figure 3, Figure 5). During wintertime (Figure 5), iodine behaves
303 similarly to sodium. Sodium does not undergo photochemical processes in the snow and is often used
304 to evaluate/correct for marine sea spray emission/deposition (Spolaor et al., 2014). During winter,
305 iodine has higher concentrations and enrichment factors (compared to its sea water abundance based
306 on the I/Na mass ratio). These higher values in surface snow could be due to the absence of
307 photochemical activation by solar radiation. In the absence of photochemistry and with limited
308 biological production in winter (Ardyna et al., 2013), we expect to find enrichment values close to
309 the seawater abundance. However, during the 2017 experiment, iodine had higher than expected
310 enrichment values suggesting that an extra source(s), in addition to sea spray emission may exist and
311 that it might be dominant during winter. Saiz-Lopez et al. 2016 suggests that night time radical
312 activation can occur. They indicate that the reaction of HOI with NO_3 , to yield $\text{IO} + \text{HNO}_3$, is possible
313 under winter tropospheric conditions (Saiz-Lopez et al., 2016). The inclusion of this reaction, along
314 with that of $\text{I}_2 + \text{NO}_3$, has a number of significant implications, such as the night time activation of
315 iodine radical chemistry that can cause an enhanced night time oceanic emissions of HOI and I_2 (Saiz-
316 Lopez et al., 2016). Sea spray aerosol droplets could absorb gas phase iodine emissions from the
317 ocean surface (as suggested by the high correlation between total iodine and sodium, Figure 5 and
318 Table 2) and deposited on the surface snow causing the high iodine surface snow enrichment. This
319 process, together with the absence of photoactivation that causes iodine loss from the snow surface,
320 could explain the high level of iodine during the polar night.



321 In parallel to iodine, our experiments have focused on the rapid changes in mercury concentrations
322 that could occur in surface snow during the polar night. This is because without these temporal
323 resolution measurements, it is extremely difficult to determine which reactions might be occurring.
324 During the first 24 hours of the winter experiment (2017) we had strong winds remodelling the snow
325 surface. Variations in surface mercury concentrations detected within the first 24 hours may in part
326 have been due to snowfall and physical artefacts caused by windblown snow redistribution. After the
327 storm, total mercury concentrations in surface snow tended to stabilize until the end of the experiment.
328 It should be noted that some oscillations in surface snow mercury concentrations and the ambient air
329 above have been detected. Mercury in the snow rapidly decreased from 00:00 on the 24th until noon
330 on the same day and was associated with an increase in the atmospheric mercury concentration
331 (Figure 5). After this sharp increase, the GEM concentration decreased rapidly while the surface snow
332 mercury increased. These two rapid events occurred within about 24 hours, supporting the idea of a
333 connection and interchange between GEM and the mercury present in snow surface, even during the
334 night-time. Night-time mercury reactions have been thought to occur. Angot et. al. 2016b suggested
335 that mercury deposition onto the snow surface in the dark could be due to several mechanisms,
336 including gas-phase oxidation, heterogeneous reactions, or dry deposition of Hg(0) (Angot et al.,
337 2016b; Song et al., 2018). This hypothesis however is based on results obtained at Dome C on the
338 Antarctic Plateau over the entire winter season, conditions very different to those in Svalbard. The
339 average mercury surface snow concentrations detected during the winter experiment are comparable
340 to those during the 2015 experiment (Figure 2 and Table 1), this might be due, as for iodine, to the
341 lack of light induced snow re-emission, but might also be caused by different background
342 concentrations independent of any seasonal effect.

343 The most interesting experiment is the one conducted during early April in 2016 when a day and
344 night cycle was still present (Figure 3). During this experiment, mercury and iodine, show a similar
345 pattern with a distinct diurnal cycle in surface snow (I_{snow} vs Hg_{snow} $R = 0.57$ $p\text{-value} < 0.01$). For
346 both elements, the highest concentrations were detected during the night and the lowest during the
347 day. Iodine has been demonstrated to be active in the upper snow layer. Previous laboratory and
348 outdoor experiments have demonstrated two photo-induced mechanisms for the release of inorganic
349 iodine from the snowpack to the atmosphere: i) photooxidation of iodide in ice with the resulting
350 production of tri-iodide (I_3^-) and evaporable molecular iodine (I_2) (Kim et al., 2016), and ii) the
351 emission of an iodine photofragments following the heterogenous photoreduction of iodate in ice
352 (Gálvez et al., 2016). These experimental studies have shown that the release of iodine from the
353 snow/ice to the atmosphere depends on solar radiation. Indeed, (Raso et al., 2017) recently measured
354 I_2 in the Arctic atmosphere under natural sunlight conditions with results that are in agreement with
355 the supposed photochemical production mechanisms.



356 Kim et al., 2016, showed that the iodide photooxidation to I_3^- strongly depended on irradiation time
357 following the UV-Visible absorption spectrum of iodide in ice. This would explain the observations
358 of reduced iodine concentrations in ice during the sunlit parts of the day. Although we do not have
359 observations of atmospheric iodine, it is very likely that snow re-emission during the day leads to a
360 peak in reactive gas phase iodine in the overlying polar boundary layer at low solar zenith angles.
361 The emitted gas phase iodine would then readily form reservoir species (HOI, $IONO_2$, HI) (Saiz-
362 Lopez et al., 2014) that once photochemistry ceases could deposit and accumulate in the snow/ice
363 until the following sunrise, when re-emission starts again.

364 Active mercury recycling from the snow pack has already been suggested/observed by several authors
365 (Dommergue et al., 2012; Durnford and Dastoor, 2011; Song et al., 2018; Steffen et al., 2008).
366 Mercury in its oxidized forms can be deposited onto the snowpack, increasing total Hg concentrations
367 in the upper snow strata. Once present in the snowpack, Hg is very labile, it can be reduced back to
368 $Hg(0)$ and can undergo dynamic exchange with the atmosphere above (Steffen et al., 2002).
369 Photochemical reactions are important in altering the speciation of Hg in the snowpack and depend
370 on environmental properties and snowpack chemistry. Spolaor et al. 2018 shows that total Hg
371 concentrations in the surface snow in the inner Antarctic Plateau do not exhibit a clear diurnal cycle
372 as has been determined for gaseous elemental mercury (Angot et al., 2016c; Dommergue et al., 2012).
373 However Hg in surface snow shows the highest values during the insolation minima, suggesting that
374 its concentration in the snow might be influenced by daily differences in incoming solar radiation.
375 The experiment at Dome C (Spolaor et al. 2018) was carried out under full polar day conditions with
376 incoming solar radiation reaching the snow surface for the entire period of the experiment. The
377 experiment conducted at Ny-Ålesund between the 6th to the 9th of April 2016 was characterized by a
378 night and day cycle. Similar to iodine, a clear diurnal cycle has been detected for atmospheric and
379 surface snow mercury. Snow mercury shows the highest concentrations during the night, with a
380 minimum during the daytime (night periods are highlighted in Figure 3 by the grey rectangular).
381 Contrary to this, the GEM shows a minimum during the nighttime and a maximum during the daytime.
382 This antiphase behaviour (Figure 3 and Table 2) suggests that under day light conditions, mercury in
383 the surface snow can be reduced and released by photochemical processes from the snow surface,
384 resulting in increases in atmospheric concentrations. During the night, mercury can be oxidized to
385 $Hg(II)$ and re-deposited onto the snow surface. In addition to this diurnal oscillation during the
386 experiment, if we exclude the snowfall that caused a re-enrichment of surface snow for both elements,
387 we detected a decreasing trend for mercury in snow as well as in the atmosphere (Figure 4 and Table
388 2), from the beginning to the end of the experiment. This decreasing trend may be ascribed to re-
389 emission during the daytime and an incomplete deposition during the night due to possible
390 dilution/removal processes caused by the surrounding atmosphere, with air mass movements as well
391 for mixing within the upper atmospheric strata. This suggested atmospheric removal could explain



392 the positive correlation between GEM and snow surface Hg seen in Table 2 that is masking the
393 antiphase caused by the diurnal daylight cycle. When the two series are de-trended by removing the
394 overall decreasing trend, (by considering 6-hour average values) the correlation between atmospheric
395 and snow mercury becomes significantly negative (Figure 4 upper panel and Table 2).

396 At the end of the 2016 experiment, a snowfall event occurred (Figure 3 pink rectangular). The net
397 effect of the snowfall was to increase the mercury concentration in the upper snow surface.
398 Precipitation events seem to be associated with elevated total Hg concentrations in surface snow
399 samples (Figure 2 and Figure 3). Angot et al., 2016c have suggested that the presence of ice crystals
400 could enhance the dry deposition of Hg(II). Indeed, due to an elevated specific surface area, the
401 mercury-capture efficiency of ice crystals is high (Douglas et al., 2008). Although there is a
402 deposition of mercury to surface snow, atmospheric mercury did not show a decrease in concomitance
403 with the snowfall but continued to show the usual diurnal pattern. In Antarctica, it has been
404 demonstrated that snow and atmospheric mercury concentrations are related but it should be taken
405 into consideration that the boundary layer can be confined to the first 30 meters above the snow
406 surface (Angot et al., 2016a). The mercury released from the snow after snowfall may not be enough
407 to impact the GEM due to dilution effects. Is also possible that the Zeppelin station is located often
408 above the marine boundary layer and the mercury released from the snow is confined and is not able
409 to influence the mercury concentration in the free troposphere. Zeppelin station is at a higher elevation
410 (approximately 400 meters above the sampling site) compared to the snow-sampling site, but is the
411 only site giving hourly mercury atmospheric measurements in the area. Although the two sites might
412 not be directly connected, the atmospheric concentrations and their diurnal cycle may be
413 representative of the atmospheric cycle above the surrounding snow field as suggest by a previous
414 study (Aspmo et al., 2005).

415 Surface snow iodine concentrations, similarly to mercury, are enhanced during liquid or solid
416 deposition. Several studies have demonstrated that rain, snow and aerosol are enriched in soluble
417 organic iodine as well as inorganic iodine (iodide and iodate) (Baker, 2005; Saiz-Lopez and von
418 Glasow, 2012). Uptake of iodine species by cloud droplets and snowflakes followed by wet
419 deposition or snowfall are major atmospheric iodine removal processes, which would enhance the
420 concentration of iodine in the snow/ice. It is interesting to note that after the snowfall events, the
421 enhanced concentrations in surface snow rapidly decrease. This phenomenon is more evident during
422 the 2015 experiment (Figure 2) when 24 hours of solar irradiation occur. In the 2016 experiment after
423 the snowfall, the iodine decrease is probably masked by nocturnal deposition. Bromine was also
424 measured during the 2016 experiment (Figure 6) to understand if, as for iodine and mercury, it can
425 undergo surface recycling. Bromine shows a correlation of $r = 0.85$ with sodium and, the Br_{enr} factor
426 (calculated as $Br_{enr} = Br_{snow} \times (Na_{snow})^{-1} \times [Br/Na]_{sw}$, where $Br/Na_{sw} = 0.006$), does not show a diurnal
427 cycle as for iodine (and its enrichment factor) and mercury. As has already been proposed, bromine



428 after deposition is probably preserved in surface snow (Spolaor et al. 2014). During snowfall, both
429 sodium and bromine decrease, most likely due to the dilution effect caused by new snowfall. It is
430 likely that the main sodium and bromine deposition occurred by sea spray deposition caused by wave
431 breaking (no sea ice was present in the fjord in front of Ny-Alesund during the experiments so the
432 bromine explosion over sea ice did not occur). Windblown snow and, eventual snowfall, can affect
433 the deposition of what is present in the atmosphere and dilute the concentrations in surface snow.
434 However, it should be noted that although Br and Na surface snow concentrations decrease during
435 snowfall, the Br enrichment factor increased, suggesting that snowfall is able to scavenge gas phase
436 bromine present in the atmosphere in addition to the aerosol phase and deposit it onto the snow surface.
437 The experiment conducted in 2015 was characterized by full light conditions (Figure 2) similar to
438 those encountered in Antarctica (Spolaor et al., 2018). Both iodine and mercury in surface snow did
439 not show any diurnal cycle suggesting that a continuous recycling process may act on the snow
440 surface. Iodine shows an almost constant concentration in the first part of the experiment with some
441 oscillations, connected to sodium variations, hence possible sea spray deposition, occurring in the
442 second part of the experiment. While GEM still shows a clear diurnal cycle, the mercury in the snow
443 does not (Figure 2). The Hg concentration in the surface snow has some variations that are not
444 connected with changes in incoming solar radiation. As for the 2016 experiment, during the last days
445 of the experiment, a snowfall occurred, causing a rapid enrichment of iodine and Hg in the surface
446 snow followed by a rapid decrease most likely due to photo induced re-emission processes.

447

448 **5. Conclusions**

449 Three high temporal resolution experiments have been carried out between 2015 and 2017. The three
450 experiments were aimed at studying the behaviour of iodine and mercury (and bromine only in 2016)
451 in snow during the different polar seasons. One was conducted during the polar night (2017), one
452 during the spring when the night and day cycle was present (2016) and one during late spring when
453 sunlight was present for 24 hours a day (2015). The results obtained show that these elements have
454 markedly different behaviours in surface snow that are mainly governed by sunlight and snow
455 deposition. For iodine, the highest snow concentrations were detected during the winter polar night
456 experiment (2017), while the lowest were during late spring (2015) when continuous solar radiation
457 reaches the snow surface. For mercury the highest concentrations were detected in the winter (2017)
458 and during late spring experiment (2015).

459 Our high temporal resolution experiments did not have the aim of characterizing the average surface
460 snow concentrations but were designed to understand the behaviour of these elements in surface snow
461 within specific seasonal changes that can occur. A clear diurnal cycle for mercury and iodine has
462 been determined when a day and night cycle was still present, however, for Br (and its enrichment
463 factor) no diurnal cycle has been detected showing it has a more conservative behaviour in snow.



464 Total mercury concentrations in surface snow peak during the night and decreases during the day, the
465 opposite of its behaviour in the atmosphere. Iodine, acts similarly to mercury, peaking during the
466 night and decreasing during the day. Considering our finding that up to 70% of the iodine present in
467 the snow can be released to the atmosphere by photo-induced reactions. the active role of snow in
468 providing gas phase iodine should be considered in studies of nucleation processes in the polar
469 atmosphere.

470 This unique set of experiments has demonstrated for the first time the different behaviours of these
471 target elements under different irradiation conditions and demonstrate that snow is an active substrate.
472 The results obtained in Arctic snow could be translated to alpine regions and, more generally,
473 anywhere in the presence of snow. The diurnal cycle determined for mercury in the Arctic, if
474 demonstrated occurring in other places with high snow cover, could have an impact on water
475 resources, with higher concentrations of mercury deposited in the water basin at night. These
476 experiments have underlined some specific processes that can occur in surface snow, however
477 additional studies are planned to better understand the real impact of these processes on the overlying
478 atmosphere.

479
480

481 **Author contribution**

482 A.S., E.B., D.C. conceived the experiment; A.S., E.B., D.C., F.G., F.D. collected the samples; A.S.,
483 C.T., F.L., E.B. measured the samples; M.M., M.Mat. provide the meteorological and radiation data;
484 K.A.P. provide the mercury atmospheric data; A.S. ASL, WRLC, HA wrote the paper with inputs
485 from A.D., C.B., M.B.

486

487 **Acknowledgements**

488 This project has received funding from the European Union's Horizon 2020 research and innovation
489 programme under grant agreement No 689443 via project iCUPE (Integrative and Comprehensive
490 Understanding on Polar Environments). We thank the support received at the Dirigibile Italia Arctic
491 Station from the National Research Council — Department of Earth System Science and
492 Environmental Technologies (CNR-DSSTTA). We acknowledge the help of ELGA LabWater in
493 providing the PURELAB Pulse and PURELAB Flex which produced the ultrapure water used in
494 these experiments.

495
496
497
498
499
500



501 **TABLES**

502 **Table 1.** Concentration of iodine and its enrichment in surface snow (I_{snow} , I_{enr}), surface snow mercury
 503 (Hg_{snow}), atmospheric mercury (Hg_{atm}) and surface snow sodium (Na_{snow}) during the different
 504 experiments. Concentrations and standard deviation (in brackets) are calculated for the entire dataset;
 505 when marked with (*) indicates that the concentration has been calculated without considering the
 506 snow fall events.

507

	I_{snow} (ngg^{-1})	Na_{snow} (ngg^{-1})	Hg_{snow} (ngg^{-1})	Hg_{atm} (ngm^{-3})	I_{enr}
2015 (day)	0.147 (0.162)	3442 (1180)	0.010 (0.006)	1.45(0.18)	10.7 (25.5)
2015*	0.090 (0.027)	3502 (1030)	0.009 (0.004)	1.46(0.19)	4.59 (1.43)
2016 (day\night)	0.167 (0.076)	2041 (777)	0.007 (0.008)	1.35 (0.13)	25.7 (46.4)
2016*	0.142 (0.057)	2317 (498)	0.007 (0.009)	1.40 (0.08)	10.2 (3.28)
2017 (night)	0.382 (0.175)	1518 (749)	0.009 (0.006)	1.26 (0.07)	44.3 (11.2)
2017*	0.433 (0.185)	1786 (770)	0.008 (0.004)	1.26 (0.06)	41.8 (8.40)

508

509

510 **Table 2.** Correlation coefficient between Iodine and sodium, bromine and sodium (only 2016) and
 511 atmospheric and snow mercury. The correlation is calculated for the entire dataset. When the
 512 correlation is marked with “*”, this indicates that the correlation has been calculated without
 513 considering the snow fall events. During the 2016 experiment the correlation between Hg_{snow} vs
 514 Hg_{atm} * has been detrended to highlight the antiphase between Hg_{atm} and Hg_{snow} . The plus and minus
 515 indicate if the association is positive or negative, which the values in parenthesis are the p-values.

516

	I vs Na	I vs Na*	Br vs Na	Br vs Na*	Hg_{snow} vs Hg_{atm}	Hg_{snow} vs Hg_{atm}*
2015	0.24 (0.052)+	0.63 (<0.01)+	NA	NA	0.18 (0.13)+	0.36 (0.011)+
2016	0.21 (0.041)+	0.62 (<0.01)+	0.91 (<0.01)+	0.74 (<0.01)+	0.12 (<0.01)+	0.43 (<0.01)**
2017	0.90 (<0.01)+	0.89 (<0.01)+	NA	NA	0.22 (0.05)+	0.062 (0.63)+

**detrended 0.61 (0.056)-

517

518

519

520

521

522

523

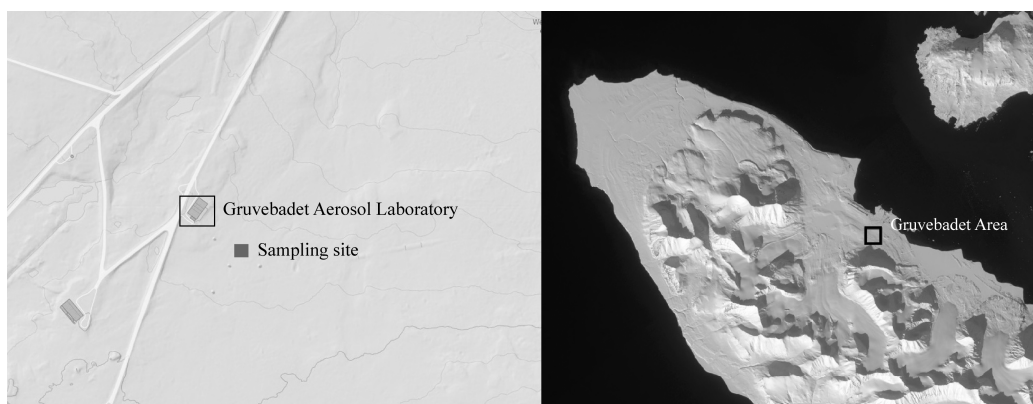


524 **FIGURES**

525

526 **Figure 1.** Location of the experimental area in the proximity of Ny-Ålesund research village (black
527 rectangular – right panel) and the site of experiments (grey rectangular – left panel) behind the
528 “Gruvebadet” Aerosol Laboratory. Maps from toposvalbard.npolar.no.

529



530

531

532

533

534

535

536

537

538

539

540

541

542

543

544

545

546

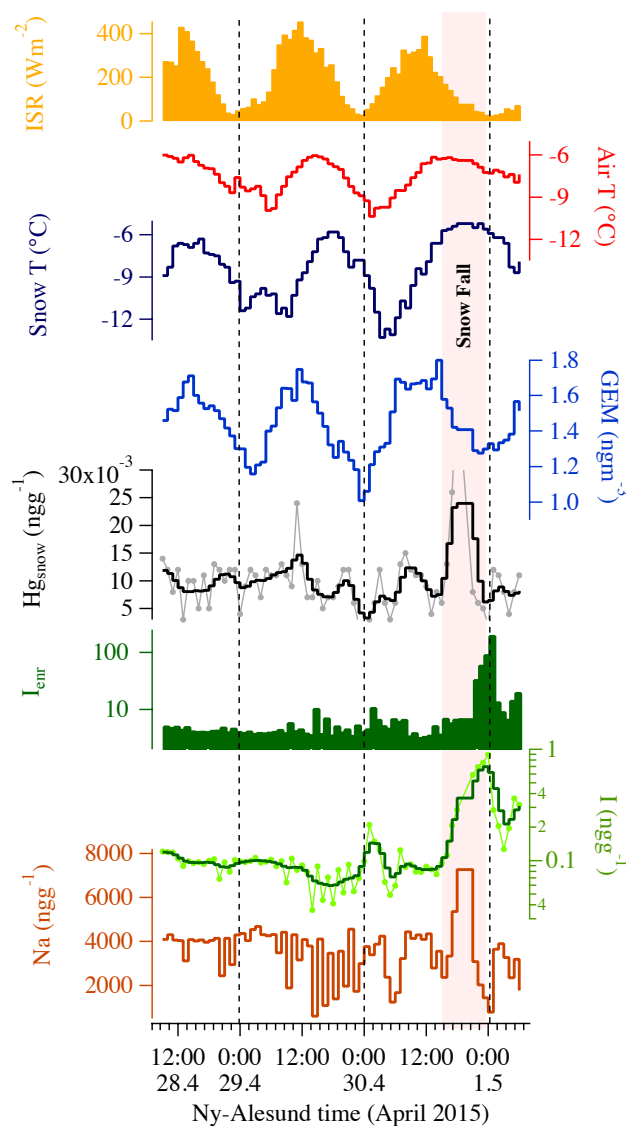
547

548

549



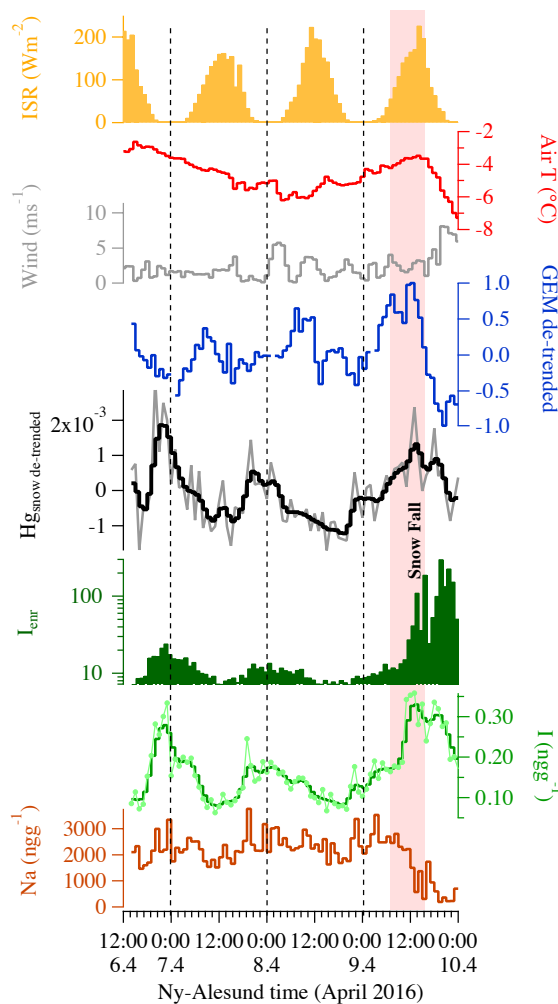
550 **Figure 2.** The 2015 experiment: continuous light conditions. The hourly sodium (dark red)
551 concentrations are connected with iodine concentrations (light green for the raw data and green for
552 the three-point smoothing) except during the snowfall where the signals decouple. Iodine enrichment
553 (dark green) demonstrates the effect of snowfall on iodine concentration in surface snow. Gaseous
554 elemental mercury (blue) exhibit a diurnal pattern while total mercury in surface snow (grey line and
555 black line three-point smoothing) does not. Snowfall occurrence is highlighted by the pink rectangle.
556 Snow and air temperature (dark blue and red) show the diurnal cycle connected with incoming solar
557 radiation (ISR - solid yellow). Wind speed is not shown since it was almost constant during the entire
558 experiment. Dashed vertical lines indicate local midnight time.



559



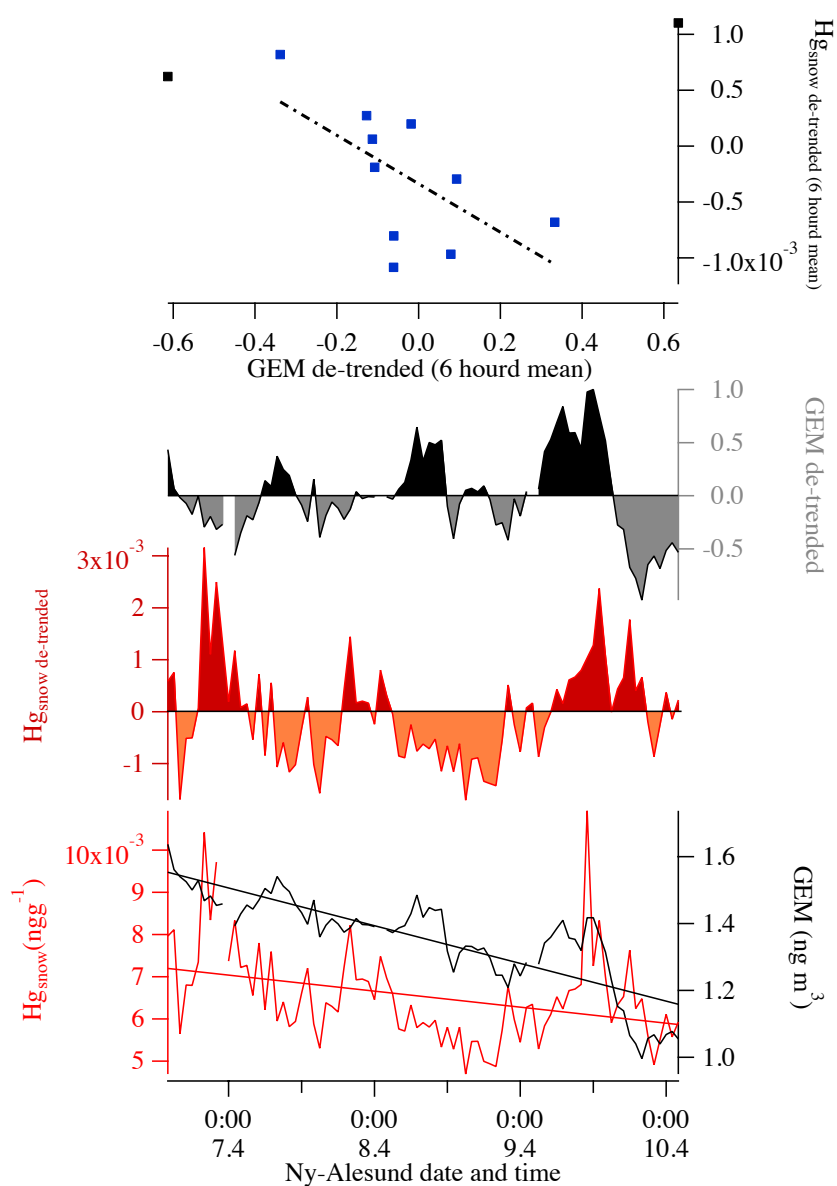
560 **Figure 3.** The 2016 experiment took place when a day and night cycle was available (night periods
561 highlighted by grey rectangular). Iodine concentration (light green line for the raw data and green
562 light for the three-point smoothing) exhibited a diurnal variability (except during the snow fall event),
563 not detected for sodium (dark red line). The Iodine enrichment factor (dark green solid line) also
564 exhibited a diurnal cycle and highlights the effect of snowfall on iodine concentration in surface snow
565 (pink rectangle shows the snow fall event). De-trended GEM (blue line) and the surface snow de-
566 trended total mercury concentrations (grey lines for raw data and black line for the three-point
567 smoothing) show opposing diurnal patterns. Additional information can be found in Figure 4. Air
568 temperature does not show a pronounced diurnal cycle (purple line) connected with incoming solar
569 radiation (ISR - yellow solid). Wind speed is shown in grey. Dashed vertical lines indicate local
570 midnight time.



571



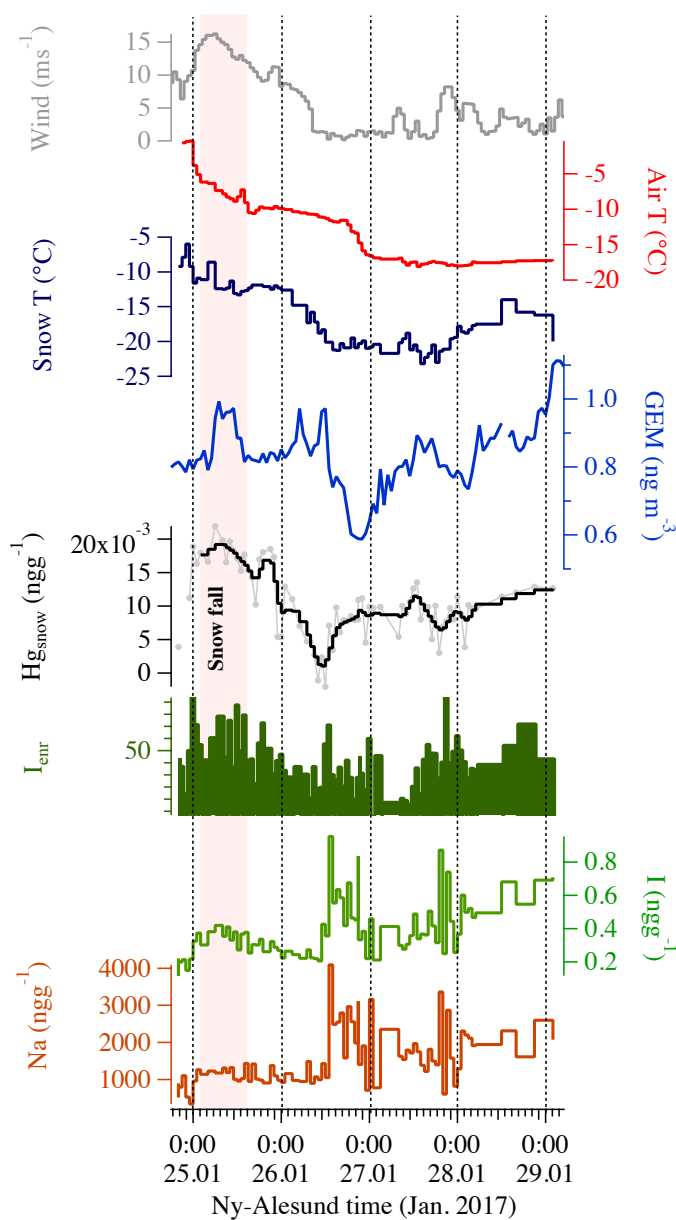
572 **Figure 4.** The lower panel shows the two series without any statistical treatment (Hg_{atm} =black;
573 Hg_{snow} =red). The regression line obtained for surface snow mercury is $Hg_{snow}=-0.0004t + 16.136$,
574 while for atmospheric mercury is $GEM=-0.1127t + 4787.8$. The middle panel shows the de-trended
575 Hg series in surface snow (in red/orange) and atmosphere (grey/black). The upper panel shows the
576 correlation between detrended Hg_{snow} and Hg_{atm} considering 6-hour average value.



577



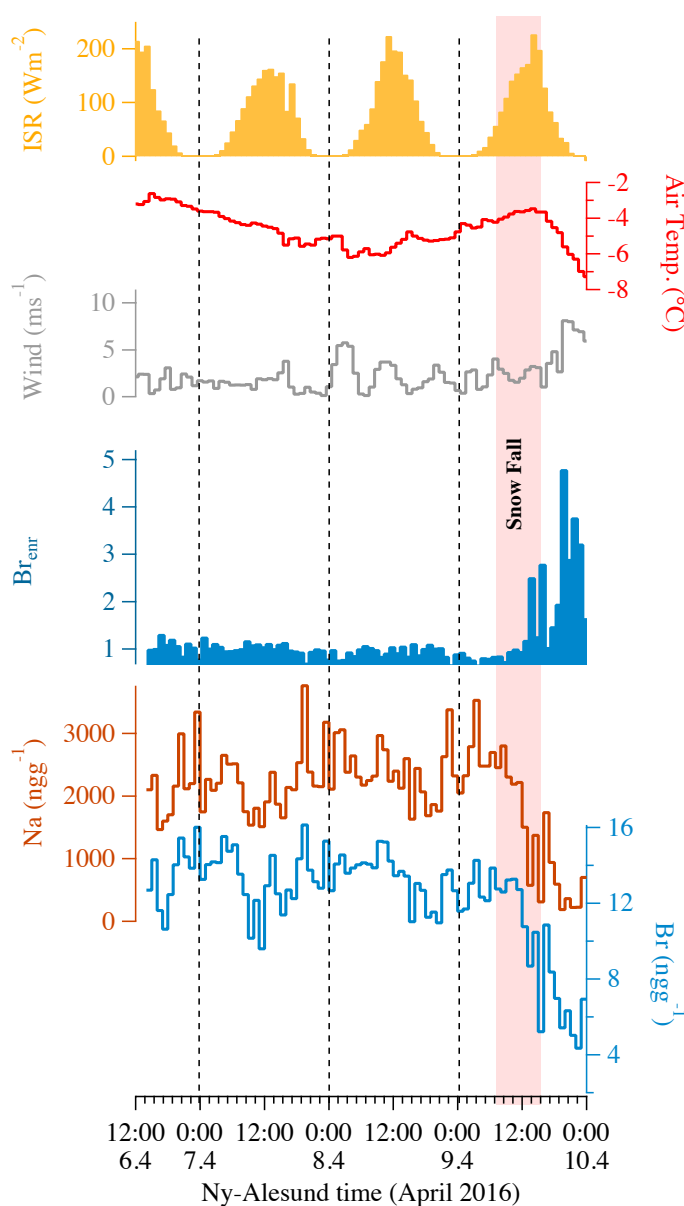
578 **Figure 5.** The 2017 experiment was conducted during the polar night. Iodine concentration (green
579 line) correlated with sodium concentration (dark red line). The Iodine enrichment factor (dark green
580 solid line) did not exhibit any diurnal cycle and had the higher value compare the three experiments.
581 Gaseous elemental mercury (blue line) and the surface snow total mercury concentrations did not
582 exhibit any diurnal pattern (light grey line for raw data and black line for three-point smoothed).
583 Snow and air temperature (dark blue and red) did not show any diurnal cycle. Wind speed is shown
584 in grey. Dashed vertical lines indicate local midnight time.



585



586 **Figure 6.** Surface Bromine recycle during the 2016 experiment. The Bromine concentration (light
587 blue line) does not show a diurnal variability and follows the sodium surface concentration (dark red
588 line). Bromine enrichment factor (blue solid line calculated as $Br_{enr} = Br_{snow} / (Na_{snow} \times 0.006)$ where
589 0.006 is the Br/Na sea water mass ratio) do not show a diurnal cycle but it is evident that snowfall
590 effects the bromine concentration and its enrichment factor during snowfall (pink rectangle). Air
591 temperatures do not show a pronounced diurnal cycle (red line) connect with the incoming solar
592 radiation (solid yellow). Dashed vertical lines indicate local midnight time.



593



594 References

- 595 Allan, J. D., Williams, P. I., Najera, J., Whitehead, J. D., Flynn, M. J., Taylor, J. W., Liu, D.,
596 Darbyshire, E., Carpenter, L. J., Chance, R., Andrews, S. J., Hackenberg, S. C., and McFiggans, G.:
597 Iodine observed in new particle formation events in the Arctic atmosphere during ACCACIA,
598 *Atmos. Chem. Phys.*, 15, 5599-5609, 2015.
- 599 Angot, H., Dastoor, A., De Simone, F., Gårdfeldt, K., Gencarelli, C. N., Hedgecock, I. M., Langer,
600 S., Magand, O., Mastromonaco, M. N., Nordstrøm, C., Pfaffhuber, K. A., Pirrone, N., Ryjkov, A.,
601 Selin, N. E., Skov, H., Song, S., Sprovieri, F., Steffen, A., Toyota, K., Travnikov, O., Yang, X., and
602 Dommergue, A.: Chemical cycling and deposition of atmospheric mercury in polar regions: review
603 of recent measurements and comparison with models, *Atmos. Chem. Phys.*, 16, 10735-10763,
604 2016a.
- 605 Angot, H., Dion, I., Vogel, N., Legrand, M., Magand, O., and Dommergue, A.: Multi-year record of
606 atmospheric mercury at Dumont d'Urville, East Antarctic coast: continental outflow and oceanic
607 influences, *Atmos. Chem. Phys.*, 16, 8265-8279, 2016b.
- 608 Angot, H., Magand, O., Helmig, D., Ricaud, P., Quennehen, B., Gallée, H., Del Guasta, M., Sprovieri,
609 F., Pirrone, N., Savarino, J., and Dommergue, A.: New insights into the atmospheric mercury
610 cycling in central Antarctica and implications on a continental scale, *Atmos. Chem. Phys.*, 16, 8249-
611 8264, 2016c.
- 612 Ardyna, M., Babin, M., Gosselin, M., Devred, E., Bélanger, S., Matsuoka, A., and Tremblay, J.-E.:
613 Parameterization of vertical chlorophyll a in the Arctic Ocean: impact of the subsurface chlorophyll
614 maximum on regional, seasonal, and annual primary production estimates, *Biogeosciences*, 10,
615 4383-4404, 2013.
- 616 Aspö, K., Gauchard, P.-A., Steffen, A., Temme, C., Berg, T., Bahlmann, E., Banic, C., Dommergue,
617 A., Ebinghaus, R., Ferrari, C., Pirrone, N., Sprovieri, F., and Wibetoe, G.: Measurements of
618 atmospheric mercury species during an international study of mercury depletion events at Ny-
619 Ålesund, Svalbard, spring 2003. How reproducible are our present methods?, *Atmospheric*
620 *Environment*, 39, 7607-7619, 2005.
- 621 Baker, A. R.: Marine Aerosol Iodine Chemistry: The Importance of Soluble Organic Iodine,
622 *Environmental Chemistry*, 2, 295-298, 2005.
- 623 Björkman, M. P., Kühnel, R., Partridge, D. G., Roberts, T. J., Aas, W., Mazzola, M., Viola, A.,
624 Hodson, A., Ström, J., and Isaksson, E.: Nitrate dry deposition in Svalbard, *Tellus B; Vol 65* (2013),
625 2013. 2013.
- 626 Björkman, M. P., Vega, C. P., Kühnel, R., Spataro, F., Ianniello, A., Esposito, G., Kaiser, J., Marca,
627 A., Hodson, A., Isaksson, E., and Roberts, T. J.: Nitrate postdeposition processes in Svalbard surface
628 snow, *Journal of Geophysical Research: Atmospheres*, 119, 12,953-912,976, 2014.
- 629 Brage B. Hansen, Ketil Isaksen, Rasmus E. Benestad, Jack Kohler, Åshild Ø Pedersen, Leif E Loe,
630 Stephen J. Coulson, Jan Otto Larsen, and Varpe, Ø.: Warmer and wetter winters: characteristics
631 and implications of an extreme weather event in the High Arctic, *Environ. Res. Lett.*, 9, 2014.
- 632 Brooks, S., Arimoto, R., Lindberg, S., and Southworth, G.: Antarctic polar plateau snow surface
633 conversion of deposited oxidized mercury to gaseous elemental mercury with fractional long-term
634 burial, *Atmospheric Environment*, 42, 2877-2884, 2008.
- 635 Cuevas, C. A., Maffezzoli, N., Corella, J. P., Spolaor, A., Vallelonga, P., Kjær, H. A., Simonsen, M.,
636 Winstrup, M., Vinther, B., Horvat, C., Fernandez, R. P., Kinnison, D., Lamarque, J.-F., Barbante,
637 C., and Saiz-Lopez, A.: Rapid increase in atmospheric iodine levels in the North Atlantic since the
638 mid-20th century, *Nature Communications*, 9, 1452, 2018.
- 639 Dall'Osto, M., Beddows, D. C. S., Tunved, P., Krejci, R., Ström, J., Hansson, H. C., Yoon, Y. J.,
640 Park, K.-T., Becagli, S., Udasti, R., Onasch, T., O'Dowd, C. D., Simó, R., and Harrison, R. M.:
641 Arctic sea ice melt leads to atmospheric new particle formation, *Scientific Reports*, 7, 3318, 2017.
- 642 Dommergue, A., Barret, M., Courteau, J., Cristofanelli, P., Ferrari, C. P., and Gallée, H.: Dynamic
643 recycling of gaseous elemental mercury in the boundary layer of the Antarctic Plateau, *Atmos.*
644 *Chem. Phys.*, 12, 11027-11036, 2012.



- 645 Dommergue, A., Ferrari, C. P., Gauchard, P.-A., Boutron, C. F., Poissant, L., Pilote, M., Jitaru, P.,
646 and Adams, F. C.: The fate of mercury species in a sub-arctic snowpack during snowmelt,
647 *Geophysical Research Letters*, 30, n/a-n/a, 2003a.
- 648 Dommergue, A., Ferrari, C. P., Poissant, L., Gauchard, P.-A., and Boutron, C. F.: Diurnal Cycles of
649 Gaseous Mercury within the Snowpack at Kuujuarapik/Whapmagoostui, Québec, Canada, *Environ*
650 *Sci Technol*, 37, 3289-3297, 2003b.
- 651 Dommergue, A., Sprovieri, F., Pirrone, N., Ebinghaus, R., Brooks, S., Courteaud, J., and Ferrari, C.
652 P.: Overview of mercury measurements in the Antarctic troposphere, *Atmos. Chem. Phys.*, 10,
653 3309-3319, 2010.
- 654 Douglas, T. A., Sturm, M., Simpson, W. R., Blum, J. D., Alvarez-Aviles, L., Keeler, G. J., Perovich,
655 D. K., Biswas, A., and Johnson, K.: Influence of Snow and Ice Crystal Formation and Accumulation
656 on Mercury Deposition to the Arctic, *Environ Sci Technol*, 42, 1542-1551, 2008.
- 657 Durnford, D. and Dastoor, A.: The behavior of mercury in the cryosphere: A review of what we know
658 from observations, *Journal of Geophysical Research: Atmospheres*, 116, n/a-n/a, 2011.
- 659 Ferrari, C. P., Gauchard, P.-A., Aspmo, K., Dommergue, A., Magand, O., Bahlmann, E., Nagorski,
660 S., Temme, C., Ebinghaus, R., Steffen, A., Banic, C., Berg, T., Planchon, F., Barbante, C., Cescon,
661 P., and Boutron, C. F.: Snow-to-air exchanges of mercury in an Arctic seasonal snow pack in Ny-
662 Ålesund, Svalbard, *Atmos Environ*, 39, 7633-7645, 2005.
- 663 Førland, E. J., Benestad, R., Hanssen-Bauer, I., Haugen, J. E., and Skaugen, T. E.: Temperature and
664 Precipitation Development at Svalbard 1900-2100, *Advances in Meteorology*, 2011, 14, 2011.
- 665 Frieb, U., Deutschmann, T., Gilfedder, B. S., Weller, R., and Platt, U.: Iodine monoxide in the
666 Antarctic snowpack, *Atmos. Chem. Phys.*, 10, 2439-2456, 2010.
- 667 Gabrieli, J., Carturan, L., Gabrielli, P., Kehrwald, N., Turetta, C., Cozzi, G., Spolaor, A., Dinale, R.,
668 Staffler, H., Seppi, R., dalla Fontana, G., Thompson, L., and Barbante, C.: Impact of Po Valley
669 emissions on the highest glacier of the Eastern European Alps, *Atmos. Chem. Phys.*, 11, 8087-8102,
670 2011.
- 671 Gálvez, Ó., Baeza-Romero, M. T., Sanz, M., and Saiz-Lopez, A.: Photolysis of frozen iodate salts as
672 a source of active iodine in the polar environment, *Atmos. Chem. Phys.*, 16, 12703-12713, 2016.
- 673 Gilfedder, B. S., Petri, M., and Biester, H.: Iodine and bromine speciation in snow and the effect of
674 orographically induced precipitation, *Atmos Chem Phys*, 7, 2661-2669, 2007.
- 675 Han, Y., Huh, Y., Hong, S., Hur, S. D., and Motoyama, H.: Evidence of air-snow mercury exchange
676 recorded in the snowpack at Dome Fuji, Antarctica, *Geosciences Journal*, 18, 105-113, 2014.
- 677 Karner, F., Obleitner, F., Krismer, T., Kohler, J., and Greuell, W.: A decade of energy and mass
678 balance investigations on the glacier Kongsvegen, Svalbard, *Journal of Geophysical Research:*
679 *Atmospheres*, 118, 3986-4000, 2013.
- 680 Kim, K., Yabushita, A., Okumura, M., Saiz-Lopez, A., Cuevas, C. A., Blaszcak-Boxe, C. S., Min,
681 D. W., Yoon, H.-I., and Choi, W.: Production of Molecular Iodine and Tri-iodide in the Frozen
682 Solution of Iodide: Implication for Polar Atmosphere, *Environ Sci Technol*, 50, 1280-1287, 2016.
- 683 Kohler, J. and Aanes, R.: Effect of Winter Snow and Ground-Icing on a Svalbard Reindeer Population:
684 Results of a Simple Snowpack Model, *Arctic, Antarctic, and Alpine Research*, 36, 333-341, 2004.
- 685 Kohler, J., James, T. D., Murray, T., Nuth, C., Brandt, O., Barrand, N. E., Aas, H. F., and Luckman,
686 A.: Acceleration in thinning rate on western Svalbard glaciers, *Geophys Res Lett*, 34, 2007.
- 687 Maturilli, M., Herber, A., and König-Langlo, G.: Climatology and time series of surface meteorology
688 in Ny-Ålesund, Svalbard, *Earth Syst. Sci. Data*, 5, 155-163, 2013.
- 689 Mazzola, M., Tampieri, F., Viola, A. P., Lanconelli, C., and Choi, T.: Stable boundary layer vertical
690 scales in the Arctic: observations and analyses at Ny-Ålesund, Svalbard, *Q J Roy Meteor Soc*, 142,
691 1250-1258, 2016.
- 692 Millero, F. J., Feistel, R., Wright, D. G., and McDougall, T. J.: The composition of Standard Seawater
693 and the definition of the Reference-Composition Salinity Scale, *Deep Sea Research Part I:*
694 *Oceanographic Research Papers*, 55, 50-72, 2008.
- 695 Moroni, B., Becagli, S., Bolzacchini, E., Busetto, M., Cappelletti, D., Crocchianti, S., Ferrero, L.,
696 Frosini, D., Lanconelli, C., Lupi, A., Maturilli, M., Mazzola, M., Perrone, M. G., Sangiorgi, G.,
697 Traversi, R., Udisti, R., Viola, A., and Vitale, V.: Vertical Profiles and Chemical Properties of



- 698 Aerosol Particles upon Ny-Ålesund (Svalbard Islands), *Advances in Meteorology*, 2015, 11,
699 2015.
- 700 Moroni, B., Cappelletti, D., Crocchianti, S., Becagli, S., Caiazza, L., Traversi, R., Udisti, R., Mazzola,
701 M., Markowicz, K., Ritter, C., and Zielinski, T.: Morphochemical characteristics and mixing state
702 of long range transported wildfire particles at Ny-Ålesund (Svalbard Islands), *Atmos Environ*, 156,
703 135-145, 2017.
- 704 Obrist, D., Agnan, Y., Jiskra, M., Olson, C. L., Colegrove, D. P., Hueber, J., Moore, C. W., Sonke, J.
705 E., and Helmig, D.: Tundra uptake of atmospheric elemental mercury drives Arctic mercury
706 pollution, *Nature*, 547, 201, 2017.
- 707 Planchon, F. A. M., Gabrielli, P., Gauchard, P. A., Dommergue, A., Barbante, C., Cairns, W. R. L.,
708 Cozzi, G., Nagorski, S. A., Ferrari, C. P., Boutron, C. F., Capodaglio, G., Cescon, P., Varga, A.,
709 and Wolff, E. W.: Direct determination of mercury at the sub-picogram per gram level in polar snow
710 and ice by ICP-SFMS, *J Anal Atom Spectrom*, 19, 823-830, 2004.
- 711 Poulain, A. J., Amyot, M., Findlay, D., Telor, S., Barkay, T., and Hintelmann, H.: Biological and
712 photochemical production of dissolved gaseous mercury in a boreal lake, *Limnology and
713 Oceanography*, 49, 2265-2275, 2004.
- 714 Raso, A. R. W., Custard, K. D., May, N. W., Tanner, D., Newburn, M. K., Walker, L., Moore, R. J.,
715 Huey, L. G., Alexander, L., Shepson, P. B., and Pratt, K. A.: Active molecular iodine
716 photochemistry in the Arctic, *Proceedings of the National Academy of Sciences*, 114, 10053, 2017.
- 717 Saiz-Lopez, A., Fernandez, R. P., Ordóñez, C., Kinnison, D. E., Gómez Martín, J. C., Lamarque, J.
718 F., and Tilmes, S.: Iodine chemistry in the troposphere and its effect on ozone, *Atmos. Chem. Phys.*,
719 14, 13119-13143, 2014.
- 720 Saiz-Lopez, A., Mahajan, A. S., Salmon, R. A., Bauguitte, S. J. B., Jones, A. E., Roscoe, H. K., and
721 Plane, J. M. C.: Boundary Layer Halogens in Coastal Antarctica, *Science*, 317, 348-351, 2007.
- 722 Saiz-Lopez, A., Plane, J. M. C., Baker, A. R., Carpenter, L. J., von Glasow, R., Gomez Martin, J. C.,
723 McFiggans, G., and Saunders, R. W.: Atmospheric Chemistry of Iodine, *Chem. Rev.*, 112, 1773-
724 1804, 2012.
- 725 Saiz-Lopez, A., Plane, J. M. C., Cuevas, C. A., Mahajan, A. S., Lamarque, J. F., and Kinnison, D. E.:
726 Nighttime atmospheric chemistry of iodine, *Atmos. Chem. Phys.*, 16, 15593-15604, 2016.
- 727 Saiz-Lopez, A., Plane, J. M. C., McFiggans, G., Williams, P. I., Ball, S. M., Bitter, M., Jones, R. L.,
728 Hongwei, C., and Hoffmann, T.: Modelling molecular iodine emissions in a coastal marine
729 environment: the link to new particle formation, *Atmospheric Chemistry and Physics*, 6, 883-895,
730 2006.
- 731 Saiz-Lopez, A., Sitkiewicz, S. P., Roca-Sanjuán, D., Oliva-Enrich, J. M., Dávalos, J. Z., Notario, R.,
732 Jiskra, M., Xu, Y., Wang, F., Thackray, C. P., Sunderland, E. M., Jacob, D. J., Travnikov, O.,
733 Cuevas, C. A., Acuña, A. U., Rivero, D., Plane, J. M. C., Kinnison, D. E., and Sonke, J. E.:
734 Photoreduction of gaseous oxidized mercury changes global atmospheric mercury speciation,
735 transport and deposition, *Nature Communications*, 9, 4796, 2018.
- 736 Saiz-Lopez, A. and von Glasow, R.: Reactive halogen chemistry in the troposphere, *Chemical Society
737 Reviews*, 41, 6448-6472, 2012.
- 738 Sherman, L. S., Blum, J. D., Johnson, K. P., Keeler, G. J., Barres, J. A., and Douglas, T. A.: Mass-
739 independent fractionation of mercury isotopes in Arctic snow driven by sunlight, *Nature Geosci*, 3,
740 173-177, 2010.
- 741 Simpson, W. R., von Glasow, R., Riedel, K., Anderson, P., Ariya, P., Bottenheim, J., Burrows, J.,
742 Carpenter, L. J., Friess, U., Goodsite, M. E., Heard, D., Hutterli, M., Jacobi, H. W., Kaleschke, L.,
743 Neff, B., Plane, J., Platt, U., Richter, A., Roscoe, H., Sander, R., Shepson, P., Sodeau, J., Steffen,
744 A., Wagner, T., and Wolff, E.: Halogens and their role in polar boundary-layer ozone depletion,
745 *Atmos Chem Phys*, 7, 4375-4418, 2007.
- 746 Sipilä, M., Sarnela, N., Jokinen, T., Henschel, H., Junninen, H., Kontkanen, J., Richters, S.,
747 Kangasluoma, J., Franchin, A., Peräkylä, O., Rissanen, M. P., Ehn, M., Vehkamäki, H., Kurten, T.,
748 Berndt, T., Petäjä, T., Worsnop, D., Ceburnis, D., Kerminen, V.-M., Kulmala, M., and O'Dowd, C.:
749 Molecular-scale evidence of aerosol particle formation via sequential addition of HIO₃, *Nature*, 537,
750 532, 2016.



- 751 Song, S., Angot, H., Selin, N. E., Gallée, H., Sprovieri, F., Pirrone, N., Helmig, D., Savarino, J.,
752 Magand, O., and Dommergue, A.: Understanding mercury oxidation and air–snow exchange on the
753 East Antarctic Plateau: a modeling study, *Atmos. Chem. Phys.*, 18, 15825-15840, 2018.
- 754 Spolaor, A., Angot, H., Roman, M., Dommergue, A., Scarchilli, C., Vardè, M., Del Guasta, M., Pedeli,
755 X., Varin, C., Sprovieri, F., Magand, O., Legrand, M., Barbante, C., and Cairns, W. R. L.: Feedback
756 mechanisms between snow and atmospheric mercury: Results and observations from field
757 campaigns on the Antarctic plateau, *Chemosphere*, 197, 306-317, 2018.
- 758 Spolaor, A., Barbaro, E., Christille, J. M., Kirchgeorg, T., Giardi, F., Cappelletti, D., Turetta, C.,
759 Bernagozzi, A., Björkman, M. P., Bertolini, E., and Barbante, C.: Evolution of the Svalbard annual
760 snow layer during the melting phase, *Rendiconti Lincei*, doi: 10.1007/s12210-015-0500-8, 2016a.
761 1-8, 2016a.
- 762 Spolaor, A., Gabrieli, J., Martma, T., Kohler, J., Björkman, M. B., Isaksson, E., Varin, C., Vallelonga,
763 P., Plane, J. M. C., and Barbante, C.: Sea ice dynamics influence halogen deposition to Svalbard,
764 *The Cryosphere*, 7, 1645-1658, 2013a.
- 765 Spolaor, A., Opel, T., McConnell, J. R., Maselli, O. J., Spreen, G., Varin, C., Kirchgeorg, T., Fritzsche,
766 D., Saiz-Lopez, A., and Vallelonga, P.: Halogen-based reconstruction of Russian Arctic sea ice area
767 from the Akademii Nauk ice core (Severnaya Zemlya), *The Cryosphere*, 10, 245-256, 2016b.
- 768 Spolaor, A., Vallelonga, P., Gabrieli, J., Martma, T., Björkman, M. P., Isaksson, E., Cozzi, G., Turetta,
769 C., Kjær, H. A., Curran, M. A. J., Moy, A. D., Schönhardt, A., Blechschmidt, A. M., Burrows, J. P.,
770 Plane, J. M. C., and Barbante, C.: Seasonality of halogen deposition in polar snow and ice, *Atmos.*
771 *Chem. Phys.*, 14, 9613-9622, 2014.
- 772 Spolaor, A., Vallelonga, P., Plane, J. M. C., Kehrwald, N., Gabrieli, J., Varin, C., Turetta, C., Cozzi,
773 G., Kumar, R., Boutron, C., and Barbante, C.: Halogen species record Antarctic sea ice extent over
774 glacial-interglacial periods, *Atmos. Chem. Phys.*, 13, 6623-6635, 2013b.
- 775 Spolaor, A., Vallelonga, P., Turetta, C., Maffezzoli, N., Cozzi, G., Gabrieli, J., Barbante, C., Goto-
776 Azuma, K., Saiz-Lopez, A., Cuevas, C. A., and Dahl-Jensen, D.: Canadian Arctic sea ice
777 reconstructed from bromine in the Greenland NEEM ice core, *Scientific Reports*, 6, 33925, 2016c.
- 778 Steffen, A., Douglas, T., Amyot, M., Ariya, P., Aspö, K., Berg, T., Bottenheim, J., Brooks, S.,
779 Cobbett, F., Dastoor, A., Dommergue, A., Ebinghaus, R., Ferrari, C., Gardfeldt, K., Goodsite, M.
780 E., Lean, D., Poulain, A. J., Scherz, C., Skov, H., Sommar, J., and Temme, C.: A synthesis of
781 atmospheric mercury depletion event chemistry in the atmosphere and snow, *Atmos. Chem. Phys.*,
782 8, 1445-1482, 2008.
- 783 Steffen, A., Schroeder, W., Bottenheim, J., Narayan, J., and Fuentes, J. D.: Atmospheric mercury
784 concentrations: measurements and profiles near snow and ice surfaces in the Canadian Arctic during
785 Alert 2000, *Atmospheric Environment*, 36, 2653-2661, 2002.
- 786 Udisti, R., Bazzano, A., Becagli, S., Bolzacchini, E., Caiazza, L., Cappelletti, D., Ferrero, L., Frosini,
787 D., Giardi, F., Grotti, M., Lupi, A., Malandrino, M., Mazzola, M., Moroni, B., Severi, M., Traversi,
788 R., Viola, A., and Vitale, V.: Sulfate source apportionment in the Ny-Ålesund (Svalbard Islands)
789 Arctic aerosol, *Rendiconti Lincei*, 27, 85-94, 2016.
- 790 Vecchiato, M., Barbaro, E., Spolaor, A., Burgay, F., Barbante, C., Piazza, R., and Gambaro, A.:
791 Fragrances and PAHs in snow and seawater of Ny-Ålesund (Svalbard): Local and long-range
792 contamination, *Environmental Pollution*, 242, 1740-1747, 2018.
- 793 Wang, J., Zhang, L., and Xie, Z.: Total gaseous mercury along a transect from coastal to central
794 Antarctic: Spatial and diurnal variations, *Journal of Hazardous Materials*, 317, 362-372, 2016.
- 795 Westermann, S., Boike, J., Langer, M., Schuler, T. V., and Eitzelmüller, B.: Modeling the impact of
796 wintertime rain events on the thermal regime of permafrost, *The Cryosphere*, 5, 945-959, 2011.
- 797 Zangrando, R., Barbaro, E., Zennaro, P., Rossi, S., Kehrwald, N. M., Gabrieli, J., Barbante, C., and
798 Gambaro, A.: Molecular Markers of Biomass Burning in Arctic Aerosols, *Environ Sci Technol*, 47,
799 8565-8574, 2013.